Halogen-Bonding Complexes Based on Bis(iodoethynyl)benzene Units: A New Versatile Route to Supramolecular Materials

Lucía González,[†,‡] Nélida Gimeno,[†,‡] Rosa María Tejedor,[§] Victor Polo,[∥] M. Blanca Ros,[†,‡] Santiago Uriel,[†,⊥] and José Luis Serrano*[,†,⊥]

[†]Departamento de Química Orgánica, Facultad de Ciencias, Universidad de Zaragoza, 50009 Zaragoza, Spain
[‡]Instituto de Ciencia de Materiales de Aragón, Universidad de Zaragoza−CSIC, 50009 Zaragoza, Spain
[§]Centro Universitario de la Defensa, Academia General Militar, 50090 Zaragoza, Spain
[∥]Departamento de Química Física, Facultad de Ciencias, Universidad de Zaragoza, 50009 Zaragoza, Spain
[⊥]Instituto de Nanociencia Aragón, Universidad de Zaragoza, 50015 Zaragoza, Spain

ABSTRACT: Iodoalkynes [1,4-bis(iodoethynyl)benzene (***p*-BIB**) and 1,3-bis(iodoethynyl)benzene (***m*-BIB**)] have been used successfully to prepare halogen bonding complexes with a range of 4-pyridine derivatives showing liquid crystalline organizations. The trimeric halogen-bonded complexes obtained from ***p*-BIB** have a rod-like structure and exhibited high order calamitic phases (SmB and G). In contrast, ***m*-BIB** gives rise to bent-shaped structures that display SmAP-like mesophases. Furthermore it was found that the presence of three and five aromatic rings in these halogen-bonding complexes promotes calamitic mesophases while seven rings are required to stabilize bent-core mesophases. The formation of halogen bonding in the complexes was confirmed by several techniques, including FT-IR, XPS, and single crystal X-ray diffraction and the strength of the bonds was evaluated by DFT calculations

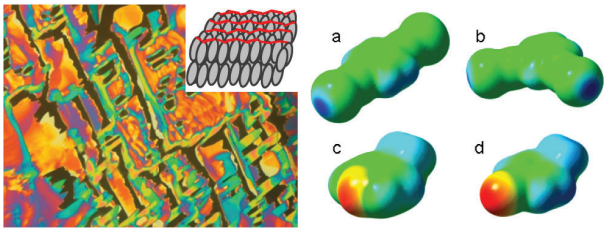

KEYWORDS: *halogen bonding, liquid crystals, supramolecular materials, bis(iodoethynyl)bencene*

Noncovalent interactions (hydrogen bonding, van der Waals forces, $\pi-\pi$ interactions, ionic interactions, etc.) have become an extraordinary and versatile tool to generate many original and attractive supramolecular architectures and functionalities in different fields. Among them, it is worth highlighting the remarkable evolution of hydrogen bonding from being a curious intermolecular interaction between a hydrogen atom and an electron-rich partner to being a powerful tool for molecular control of protein and DNA chemistry and crystal engineering of solid-state materials and also in soft matter assemblies. Regarding soft materials, the use of hydrogen bonding is quite widespread in the field liquid crystals, in which it has been successfully used to prepare functional materials with varied mesomorphic organizations.[1−3] Although pioneering studies were focused on preparing calamitic and discotic hydrogen-bonded liquid crystals,[4,5] bent-shaped liquid crystals have recently been obtained using this strategy.[6−13]

In this context, an alternative working strategy to hydrogen bonding (HB) is halogen bonding (XB). Indeed, a great deal of research has recently been carried out with the aim of understanding and harnessing this type of noncovalent interaction, which involves pairing a halogen atom with an electron-rich partner. Although the halogen bond was described more than 150 years ago,[14,15] it was not until the 1970s that Hassel highlighted the ability of this interaction to manage self-assembly processes.[16−18] During the past decade, many applications of halogen bonding in fields as diverse as crystal engineering, enantiomer separation, biology, and supermolecular architectures have been reported and reviewed.[19−24] This noncovalent interaction exhibits similar characteristics to HB in directionality and strength and may cooperate with or prevail over HB.[25]

Interestingly, the halogen bond has also recently been used in materials science, for example, to induce liquid crystal organizations. Xu, Bruce, and Metrangolo took advantage of the interaction between iodine atoms found in perfluorinated benzenes or perfluoralkanes and basic amine/imine nitrogens to prepare mesomorphic species.[25−30] These complexes, prepared as dimeric,[25,30] trimeric,[27,31,32] or polymeric[26] species, have an elongated shape that gives rise to calamitic liquid crystals. Pioneering studies were carried out on halogen-bonded systems with three or four aromatic-ring dimeric complexes bearing a stilbene derivative and a perfluoroiodobenzene. These compounds afforded nematic and SmA mesophases in all cases. More complex structures were obtained by preparing trimeric materials. Different flexible or rigid structures bearing two donor positions, i.e., two iodine atoms, have been bonded to

Scheme 1. Chemical Structures of Halogen-Bonding Donors and Acceptors Used in This Work and General Structure of the Halogen Bonded Complexes Synthesized

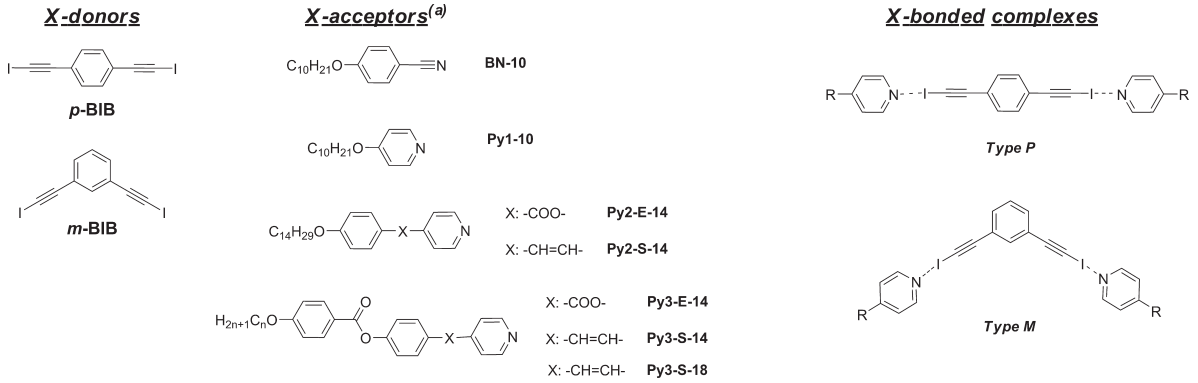

[a]**BN-10** benzonitirle derivative; **Py1-10** pyridine derivative; **Py2-E-14** two aromatic rings, ester derivative, *n*-tetradecyloxy chain; **Py2-S-14** two aromatic rings, stilbene derivative, *n*-tetradecyloxy chain; **Py3-E-14** three aromatic rings, ester derivative, *n*-tetradecyloxy chain; **Py3-S-14** three aromatic rings, stilbene derivative, *n*-tetradecyloxy chain; **Py3-S-18** two aromatic rings, stilbene derivative, *n*-octadecyloxy chain.

two stilbene derivatives and in most cases nematic materials were obtained regardless of the rigidity and linearity of the central unit. Moreover, if both ditopic donors and acceptors are employed, polymeric materials are obtained that show only a monotropic nematic phase. In these studies the fluorine atoms improve the electron acceptor ability of both diiodotetrafluorobenzene[27,30] and diiodoperfluoro-alkane[29] derivatives.

A different approach to improve the complexation ability is to attach an iodine atom to an acetylene unit. Indeed, in the early 1980s iodoacetylenes were among the first halogen-bond donors studied in solution by Laurence et al.[33−35] Despite the fact that iodoacetylenes behave as strong Lewis acids due to the I−C_{sp} bond, they have been mostly ignored in supramolecular chemistry until recent applications in the design of conducting organic crystals[36,37] and the synthesis of highly organized conjugated polymers[38−40] and molecular rotors.[41] In addition, in comparison with other diiodotetrafluorobenzene derivatives, the iodine atom, in the di(iodoethynyl)benzene derivatives, is more accessible to establish noncovalent interactions and the triple bonds extend the stiffness of the molecules, increasing the distance between the iodine atoms.

Herein, we report the preparation and characterization of halogen-bonded complexes based on bis(iodoethynyl)benzene derivatives and basic nitrogen-containing molecules with the aim of obtaining liquid crystalline materials (see Scheme 1). For all the above, the use of bis(iodoethynyl)benzene derivatives as XB-donors can favor liquid crystalline arrangements and give rise to mesophases different than those described to date for XB complexes

Two new series of halogen-bonded complexes based on linear ***p*-BIB** (series **P**) and bent ***m*-BIB** (series **M**) donors have been prepared and fully characterized. Two different types of acceptors were assayed: A benzonitrile derivative with an N_{sp} atom, the nitrogen of a nitrile group (**BN-10**), and some pyridine derivatives with an N_{sp^2} atom (**Py1-10**, **Py2-E-14**, **Py2-S-14**, **Py3-E-14**, **Py3-S-14**, and **Py3-S-18**).

In all cases, trimeric complexes based on one bis(iodoethynyl)benzene and two nitrile or pyridine derivatives were prepared. Depending on the positions of the iodoethynyl substituents in the donor ring, complexes with two different geometries are expected, i.e., rod-like complexes (for 1,4-substitution) and bent-shaped complexes (for 1,3-substitution). These complexes would be expected to give calamitic and bent-core liquid crystalline behavior, respectively. Formation of halogen bonding in the complexes was confirmed by several techniques, such as Fourier transform infrared spectroscopy (FT-IR), X-ray photoelectron spectroscopy (XPS), and single crystal X-ray diffraction (XRD). The strengths of the bonds were evaluated by DFT calculations. The thermal properties of the complexes were studied by polarized optical microscopy (POM), differential scanning calorimetry (DSC), thermogravimetric analysis (TGA), and XRD. In most cases liquid crystalline materials were obtained, even when the building blocks were not mesogenic in their own right.

RESULTS AND DISCUSSION

Synthesis. The general synthetic procedures to prepare thedifferent XB-donors and XB-acceptors are outlined in Schemes S1 and S2 of the Supporting Information. It should be pointed out that an alternative to the recently published[42] synthetic procedure for the preparation of ***p*-BIB** and ***m*-BIB** is reported. Among the differences, *N*-iodosuccinimide and silver nitrate are used as reagents and yields up to 80% are achieved. On the other hand, the synthesis and characterization of a number of XB-acceptors (**Py2-E-14**, **Py3-E-14**, **Py3-S-14**, and **Py3-S-18**) is also included.

The XB-complexes were obtained according to the method reported by Gimeno et al.[6] for the preparation of HB-complexes. XB-complexes were prepared by mixing the two components in a 1:2 stoichiometry in chloroform and stirring the mixture at room temperature until the solvent had evaporated. The resulting solid was dried under vacuum for 2 h at room temperature. The new halogen-bonded complexes reported here are identified using a notation system in which the XB-donor (**P** or **M**) and XB-acceptor are included as depicted in Scheme 1. For example, **P-Py3-E-14** is the complex of series **P**, formed from the XB-donor **P** and the XB-acceptor **Py3-E-14**.

FT-IR and XPS Spectroscopy. The formation and strength of halogen-bonding interactions in the neat materials were investigated by FT-IR and XPS spectroscopies. Intermolecular X-bond formation results in the perturbation of electron density at the associated atoms and subsequently induces a

change in its infrared (IR) vibration frequency and the X-ray photoelectron spectroscopy (XPS) binding energy.

As reported in the case of the pyridine derivatives, up to three characteristic stretching bands appear in the IR spectra in the range 1540−1640 cm^{-1}, and these are related to the pyridine skeleton. Among them, the band at ca. 1586 cm^{-1} is known to be the most sensitive, shifting to higher wavenumbers due to interactions, e.g., a large shift to ca. 1640 cm^{-1} due to protonation by strong acids, a smaller shift to ca. 1620 cm^{-1} due to metal coordination, a relatively small shift to ca. 1604 cm^{-1} due to phenolic hydrogen bonding,[43,44] and a very small shift to ca. 1593 cm^{-1} due to halogen bonding.[27]

Analysis of the IR spectra of the XB-acceptors and the complexes in the appropriate wavenumber range shows the three characteristic bands of the pyridine skeleton (see Figure 1 and Figure S1−S5 in Supporting Information). The blue shift of some of these bands in the complexes (with respect to the unbonded XB-acceptors) confirms the formation of the halogen bond (see Table S1 in Supporting Information). However, some differences that depend on the groups linked to the pyridine ring should be pointed out.

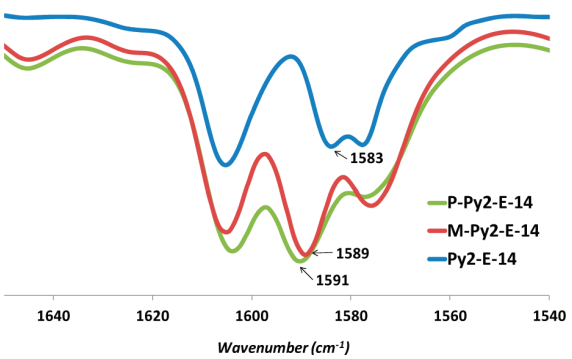

Figure 1. FT-IR (neat samples) of **Py2-E-14** (blue), **P-Py2-E-14** (green), and **M-Py2-E-14** (red).

For the stilbene derivatives, only a small blue shift (2−4 cm^{-1}) of the central band is observed, which is in accordance with the data previously reported for the same type of compound.[28] A blue shift of up to 6−8 cm^{-1} is observed for the pyridine ester complexes (e.g., from 1583 cm^{-1} in **Py2-E-14** to 1589 cm^{-1} in **M-Py2-E-14** or 1591 cm^{-1} in **P-Py2-E-14**, see Figure 1). Slightly different behavior was observed for **Py1-10**. In this case, the bands are initially red-shifted with respect to the other pyridine analogues (1593, 1579, and 1569 cm^{-1}), and upon complexation the two bands at higher wavenumber shift by between 8 and 10 cm^{-1}. Thus in the case of **M-Py1-10**, the bands are shifted from 1593 to 1601 cm^{-1} and from 1579 to 1589 cm^{-1}. A correlation is observed between the pyridine band wavenumber in unbonded XB-acceptors and the shift of the same band in the complexes. The band is shifted to a lower wavenumber in the unbonded XB-acceptor band and a larger shift is observed in the corresponding band of the complex.

Finally, for the complex based on **BN-10** a blue shift (of around 10 cm^{-1}) of the nitrile group stretching mode was observed, and this is associated with the formation of halogen bonding between nitrogen and iodine atoms.

XPS is also an effective spectroscopic method to investigate intermolecular interactions, such as ionic and H-bonding interactions, due to changes in binding energy.[27,45,46] Thus, we examined and compared the XPS spectra of selected X-bonded complexes and their corresponding unbonded components. The XPS spectra of XB-complexes of series **P** and **M**, with XB-acceptors **Py2-S-14**, **Py3-S-14**, and **Py3-S-18**, were compared. The binding energies for the I3d doublet and N1s are gathered in Table S2 in the Supporting Information.

In all complexes, a shift to lower energy is observed for the I3d doublet signal (from 0.08 to 0.41 eV) and to higher energy for N1s (from 0.73 to 1.16 eV) with respect to the value of the pure compound (see Figure 2). These changes are indicative of

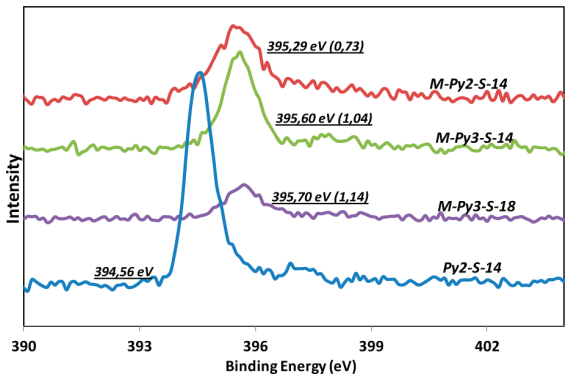

Figure 2. N1s core-level X-ray photoelectron spectra of pristine **Py2-S-14** (blue) and M-type X-bonded complexes with **Py2-S-14** (red), **Py3-S-14** (green), and **Py3-S-18** (purple).

halogen bonding formation between the constituents. The binding energy shifts of N1s are greater than those described in the literature for similar interactions.[27,46,47] The I3d binding energy shifts for the complexes with respect to their corresponding unbonded species (ca. 0.14 eV) are smaller than those described in the literature (ca. 0.30 eV).[27] In order to explain this difference, we calculated the energy of the of halogen bonding between iodine and the carbon−carbon triple bond (−5.1 kcal/mol) present in unbonded ***p*-BIB**[48] (Table 2). This value is less than those calculated for the halogen bonded complexes but is similar to values for weaker halogen-bonding interactions. This may explain the differences in the I3d binding energy shifts as iodine in benzene derivatives is not involved in halogen bonding interactions.

Liquid Crystal Properties of the Complexes. All of the XB-complexes were first studied by POM. The solid samples should melt cleanly without the appearance of biphasic regions, which would indicate a phase separation into the two individual components on heating or the presence of nonstoichiometric complexes. Unfortunately, all attempts to prepare suitable samples of complex **P-BN-10** were unsuccessful and only samples which showed inhomogeneous melting were obtained. Therefore, **P-BN-10** complex is not discussed in this section.

The thermal properties of the new materials were determined by polarizing optical microscopy (POM), differential scanning calorimetry (DSC), thermogravimetry (TGA), and X-ray diffraction (XRD) in the mesophase. The TGA characterization confirmed that the complexes are stable and weight losses (around 20%) start at similar temperatures to those observed by POM and DSC for the decomposition processes. The thermal properties of the XB-donors, XB-acceptors, and thermally stable XB-complexes are gathered in Table 1.

All of the building blocks—both XB-donors and XB-acceptors—are either liquid or crystalline, except for the

Table 1. Thermal Properties of Halogen-Bonding Donors, Acceptors, and Trimeric Halogen-Bonded Complexes

compound/ complex	phase transition temperature, °C [enthalpy, kJ mol^{-1}][a,b]
***p*-BIB**	Cr 129 [7.6] I[c]
***m*-BIB**	Cr 88 [12.8] I[c]
BN-10	Cr 31 [38.2] I
Py1−10	I (rt)
Py2-E-14	Cr 75 [48.0] I
Py2-S-14	Cr 89 [60.9] I
Py3-E-14	Cr 124 [65.8] SmA 139 [6.2] I
Py3-S-14	Cr 108 [44.2] SmA 172 [6.4] I
Py3-S-18	Cr 109 [49.8] SmA 168 [6.4] I
P-Py1-10	Cr 91 G 100 [81.7][d] I
P-Py2-E-14	Cr 87[18.9] SmB 109[e] [50.5] I
P-Py2-S-14	Cr 84 [2.6] Cr′ 105.3 [3.8] G 151.8 [77.9] dec.[c]
M-Py1-10	Cr 53 [52.5] I
M-Py2-E-14	Cr 68 [70.9] I
M-Py2-S-14	Cr 111 [87.5] I
M-Py3-E-14	Cr 120 [93.0] SmAP-like[f] 133 [5.4] I
M-Py3-S-14	Cr 107 [61.1] SmAP-like[f] 159 I[c,g]
M-Py3-S-18	Cr 101 [100.2] SmAP-like[f] 164 [12.6] I

[a]Onset values for transitions observed in the second scan at 10 °C min^{-1}. [b]Cr: crystalline phase, SmB: smectic B phase, G: G crystal phase, SmAP: smectic A polar-like phase, I: isotropic liquid. [c]First scan data as the sample decomposed on reaching the isotropic liquid. [d]Combined enthalpy of two transitions. [e]Maximum of a broad peak. [f]Lamellar orthogonal polar mesophase similar to liquid crystal phases reported for bent-core compounds. [g]Enthalpy could not be measured due to decomposition of the sample.

pyridine derivatives containing three aromatic rings, which show a SmA mesophase. It can be seen that at least three aromatic rings are needed for these new mesogenic units to induce mesomorphism as both ester and stilbene derivatives with only two aromatic rings are not liquid crystals. On the other hand, if we compare three-ring systems, the stilbene derivatives promote stronger stabilization of the SmA mesophase in comparison with the ester analogue. This may be due to the stilbene derivatives preferentially adopting a flat conformation, in contrast to the ester derivatives.

Regarding the complexes, the mesomorphic behavior depends strongly on the type of XB-donor used. Complexes in series **P** preferentially showed traditional calamitic mesophases. In this case, mesomorphism is already favored by short acceptors, either with one or two aromatic rings. All the complexes with longer acceptors (**P-Py3-E14**, **P-Py3-S-14**, **P-Py3-S-18**) yield liquid crystalline materials that decomposed before reaching the isotropic liquid. However, for Type **M** materials, mesomorphism was only observed for the longest XB-acceptors, i.e., those bearing at least seven aromatic rings in the complex. (Some representative DSC curves are gathered in Supporting Information section S4).

Series P (Rod-Like Structures). The three complexes in this series are mesomorphous. Indeed, complexes **P-Py1-10**, **P-Py2-E-14**, and **P-Py2-S-14**, with three or five aromatic rings, showed high order mesophases. To date most of the liquid crystals based on halogen bonding have shown low order calamitic mesophases such as nematic and smectic A.[27,30]

The mesophase of the shortest complex, **P-Py1-10**, was assigned as crystal G, as it showed the characteristic texture of this phase (dentritic grown of elongated platelets that are rectangular in shape) (Figure 3 (left)).[48] This phase is highly

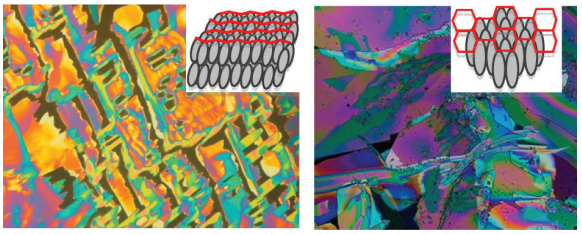

Figure 3. Optical textures of (left) G phase of **P-Py1-10** at 86 °C and (right) SmB phase of **P-Py2-E-14** at 108 °C.

viscous and showed an X-ray pattern with several sharp peaks that are characteristic of the high order of this phase (see Supporting Information). The same type of mesophase was assigned for complex **P-Py2-S-14** based on the similiraty of textures observed by POM, with rapid cooling of the sample from the isotropic liquid to minimize decomposition.

On the other hand, the other complex (**P-Py2-E-14**) showed a different mosaic texture, which in this case pointed to an SmB mesophase (Figure 3 (right)).[49] The crystalline nature of this phase was also confirmed by XRD, as a difusse halo was not observed but a couple of sharp reflections were apparent.

Both SmB and crystal G are high order phases that are more ordered than the SmA mesophase found in the XB-accpetors. In particular, in the SmB phase the molecules exhibit a hexagonal ordering within the orthogonal layers. In contrast, the crystal G phase is one of the so-called tilted soft crystal phases. This phase is even more ordered and shows long-range positional order in three dimensions, with the molecules tilted within the layers. Such high order arrangements are quite common in rod-like hydrogen-bonded complexes.[50] Furthermore, it has been claimed that these compounds have attractive optical applications,[51,52] for example, as hosts in highly ordered host−guest systems for polarizers.

Series M (Bent-Shaped Structures). Six complexes bearing ***m*-BIB** as the XB-donor were prepared and characterized. However, only the longest compounds, which contain seven aromatic rings, afforded mesomorphic materials. The other materials—with either three (**M-Py1-10**) or five (**M-Py2-E-14** and **M-Py2-S-14**) aromatic rings—did not yield liquid crystalline phases. Regarding seven-ring systems, those based on stilbene receptors (**M-Py3-S-14** and **M-Py3-S-18**) show wide mesophase ranges at relatively high temperatures. Even in cases where the textures observed in the heating process were not clear, XRD experiments allowed us to assign the type of mesophase. Up to two sharp reflections in the small-angle region and a diffuse halo in the wide-angle region were detected, thus confirming the mesomorphic nature of the phase. The presence of two or more reflections is not common in classical SmA phases but is usually found in XRD diffractograms of the SmAP phase, which was recently found in bent-core liquid crystals (see Supporting Information). Moreover, layer spacings of 79.2 Å and 89.6 Å were measured for **M-Py3-S-14** and **M-Py3-S-18**, respectively. These values are in the range of the molecular lengths calculated theoretically using Chemsketch (84 and 92 Å) for the trimeric complexes in all-trans conformations, indicating an orthogonal arrangement of the molecules within the mesophase and, hence, an orthogonal mesophase. In addition, these values are much higher than the layer spacings measured for the corresponding X-B acceptors **Py3-S-14** and **Py-3-S-18** in the SmA phase (38.5 Å and 44.6 Å, respectively). Decomposition of the material on

reaching the isotropic state precluded further observation of the textures or study under an electric field. A higher stability was observed in the case of the complex **M-Py3-E-14**, which contains an ester linking unit. Interestingly, this structural change again induced significant destabilization of the mesophase and led to lower clearing temperatures and a narrow mesophase range. However, this characteristic did enable us to study the material in the cooling process, with a typical fan-shaped texture observed with homeotropic zones. This texture is characteristic of the SmA phase (Figure 4).

Figure 4. Fan-shaped optical texture and proposed orthogonal arrangement of the SmAP-like mesophase exhibited by complex **M-Py3-E-14** at 131 °C. Black areas correspond to homeotropic regions of the sample.

It was possible to fill 5-μm ITO (indium tin oxide)-coated cells in order to study the behavior of the compounds under electric fields. Even when the material showed some instability under high electric fields, upon the application of moderate voltages, molecular switching could be detected, thus indicating polar organization in the material. A peak was not observed in the polarization current curve, probably due to the low stability of the sample. Nevertheless, based on these results and the XRD data, which suggest a compact packing, we identified the mesophase as an SmAP-like mesophase.[53] The SmAP phase is a polar variation of the SmA phase. This polar orthogonal phase was first reported for a bent-shaped molecule in 2001.[49] Several variations of this polar nontilted phase have since been reported ($SmAP_R$, $SmAP_{AR}$, SmA_dP_A, etc.)[50−55] and they are still a topic of intensive study. The good alignment observed for SmAP mesophases together with the fast response of this phase under electric fields has confirmed them as promising candidates for display applications.

Halogen bonds have been used previously to induce bent-core structures, although only calamitic mesophases have been claimed.[32] Interestingly, our results show that XB-complexes can be considered as an attractive alternative to H-bonding complexes to induce bent-core mesophases.

In an effort to gain a better understanding of the different ability of these series of complexes to form liquid crystal phases, further studies on some XB-complexes were carried out. The crystalline packing of **P-Py1-10** and **P-BN-10** was studied and modeling approaches were applied to simpler analogues (**P-Py1-1**, **M-Py1-1**, and **P-BN-1**). Details and results of these studies are reported in the following sections.

Crystal and Molecular Structure. Complexes **P-Py1-10** and **P-BN-10** crystallize in a triclinic system and their structures were solved in the centrosymmetric space group $P\bar{1}$. Crystallographic data for complexes **P-Py1-10** and **P-BN-10** are gathered in Table S3 in the Supporting Information. The asymmetric unit contains a molecule of nitrogen base and half-molecule of ***p*-BIB**, the center of which is located at an inversion center. The alkoxy chains adopt a perfect all-trans linear arrangement and are coplanar with the aromatic rings. The bond distances and angles of ***p*-BIB** are similar to those described for unbonded ***p*-BIB**[48] and small differences will be discussed in terms of X bondings.

The ***p*-BIB** acts as a bidentate XB-donor and is pinned to its binding sites by two nitrogen bases, which in turn act as monodentate electron-donors (Figure 5). The distance

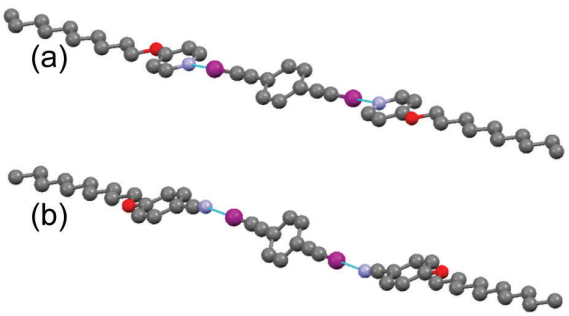

Figure 5. X-ray structures of trimeric **P-Py1-10** (a) and **P-BN-10** (b) halogen-bonded complexes. Hydrogen atoms have been omitted for clarity.

between the nitrogen and the iodine is 2.757 Å in **P-Py1-10** and 2.946 Å in **P-BN-10**. These distances correspond to a reduction of approximately 22% and 16%, respectively, of the sum of the van der Waals' radii of N and I (3.53 Å). The N···I—C angles are almost linear (172.9 and 176.4°, respectively). These experimental values match very well with the calculated distances and angles (Table 2). The longest N···I distance in **P-BN-10** indicates a lower strength for the noncovalent interaction. The difference between halogen bonding angles may be attributed to the steric hindrance—the nitrile group is less hindered as it is easier to approach by the most favorable direction. Angles found in other crystal structures of diiodotetrafluorobenzene trimeric complexes are in the range 171.2−176.7°.[30]

In the structure of **P-Py1-10**, the pyridine rings are coplanar and twisted with respect to the ***p*-BIB** plane by 20.6°. The trimers do not establish interactions with each other and they are arranged in planes. The distance between parallel planes is 3.2 Å. The supramolecular arrangement in **P-BN-10** is quite similar to that described for **P-Py1-10**. In this case the benzonitrile rings that form the trimer are staggered (1.5 Å) and rotated (32.5°) with respect to the central ***p*-BIB** ring, and finally, the distance between parallel planes is 3.7 Å.

These data, and in particular the longer N···I distance for **P-BN-10** [2.946(1) Å versus 2.757(1) Å for **P-Py1-10** showing weaker noncovalent interactions in the former], support the differences between these two types of complexes in terms of their thermal stability.

Theoretical Modeling. In order to verify theoretically the occurrence, nature, and strength of the halogen-bonding interactions, the complexes **P-Py1-1**, **M-Py1-1**, and **P-BN-1** were considered as model systems, with the decyloxy substituents replaced by methoxy groups. Complex ***p*-BIB** was also optimized in order to evaluate the interaction between the iodine and the π-electrons of the carbon−carbon triple

Table 2. Interaction Energies (ΔE_{int}), Basis Set Superposition Errors (BSSE), and Halogen Bonding Distances ($D_{I\cdots N}$) and Angles ($Z_{C-I\cdots N}$) of the Complexes[a]

partner/complex	ΔE_{int} (kcal/mol)	BSSE (kcal/mol)	$D_{I\cdots N}$ (Å)	D_{C-I} (Å)	$Z_{C-I\cdots N}$ (deg)	q_N (e)	q_I (e)	$V_{s,min}$ (kcal/mol)	$V_{s,max}$ (kcal/mol)
Py1-1						−0.468		−31.0	
BN-1						−0.317		−33.7	
***p*-BIB**				1.999			0.352		24.6
***m*-BIB**				2.000			0.350		24.7
P-Py1-1	−20.0	1.9	2.906	2.028	179.9	−0.517	0.346		
M-Py1-1	−20.0	1.7	2.890	2.029	178.6	−0.518	0.342		
P-BN-1	−15.0	1.1	3.095	2.012	179.2	−0.370	0.368		
complex ***p*-BIB**	−5.1	1.7							

[a]Bond length of the C−I bond and NBO charges of N, q_N, and I, q_I, of the partners and complexes. Partners and complexes optimized at the B98/6-311$^+$G(d,p)-DGDZVP level of theory.

bond. The calculations were carried out using the B98 exchange and correlation functional combined with the DGDZVP basis set for iodine and the 6-311+G (d,p) basis set for the other atoms. All structures were geometrically optimized in gas-phase conditions and characterized using frequency analysis. The electrostatic potential of the complex partners 4-methoxypyridine (**Py1-1**) and 1,4-methoxybenzonitrile (**BN-1**), ***p*-BIB**, and ***m*-BIB** are shown in Figure 6. The sigma-hole in the XB-donors, created by the anisotropic distribution of electronic density around the iodine atom, can be seen. Key features of the B98-calculated geometries and the interaction energies between the XB-donors and XB-acceptors are gathered in Table 2. The calculated noncovalent bonding angles $Z_{C-I\cdots N}$ are almost linear (179.9° in **P-Py1-1** and 179.2° in **P-BN-1**), and the halogen-bonding distances $D_{I\cdots N}$ (2.906 Å in **P-Py1-1** and 3.095 Å in **P-BN-1**) are appreciably shorter than the sum of the van der Waals radii (3.53 Å). These data show good agreement with angles (172.95° in **P-Py1-10** and 176.45° in **P-BN-10**) and halogen-bonding distances (2.757 Å in **P-Py1-10** and 2.946 Å in **P-BN-10**) determinated in the crystal structures of **P-Py1-10** and **P-BN-10**. The C—I bond distances increase upon the halogen-bonding complex formation.

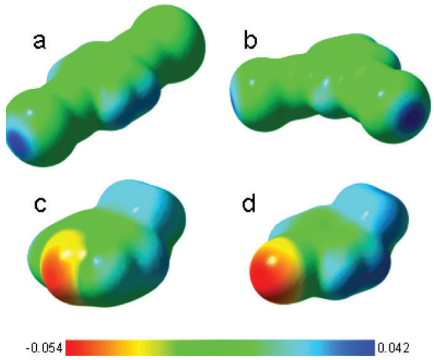

Figure 6. Computed electrostatic potential of the minimized halogen-bonding donors and acceptors (a) ***p*-BIB**, (b) ***m*-BIB**, (c) **Py1-1**, and (d) **BN-1**.

The interaction energies (ΔE_{int}) were determined using the equation:

$$\Delta E_{int} = E_{complex} - \sum E_{partner}$$

with values of −20.0 kcal/mol obtained for complexes **P-Py1-1** and **M-Py1-1** and −15.0 kcal/mol for the **P-BN-1**. These values are higher than those calculated for some analogous pyridine-halotetrafluorobenzene complexes[27,47,56] and are in the typical range for medium-to-strong hydrogen bonding.[57] Furthermore, these energies depend on the halogen-bonding acceptor, with pyridine complexes showing higher interaction energies than the nitrile complex. In addition, the I···N distance of the trimers **P-Py1-1** and **M-Py1-1** is shorter than the analogous distance of the complex **P-BN-1**. This fact is consistent with the nitrogen of the pyridine derivate enhancing the halogen bonding appreciably.

The presence of a sufficiently strong positive region on the outer surface of an atom is an indication that an attractive interaction with a nucleophile is likely, although this is not the only factor. The values of the most positive electrostatic potentials on the molecular surfaces ($V_{s,max}$) for ***p*-BIB** and ***m*-BIB** (24.6 kcal/mol) are similar to that of 1,4-diiodotetrafluorobenzene (23.2 kcal/mol). Despite this, the interaction energies calculated for the complexes **P-Py1-1** and **M-Py1-1** (ΔE_{int} = −10 kcal/mol) are higher than those described for 1,4-diiodotetrafluorobenzene with pyridine derivatives (ΔE_{int} = −5.59 kcal/mol).[56] This may be due to combination of a higher $V_{s,max}$ and the lower steric hindrance of di(iodoethynyl)benzene derivatives.

CONCLUSIONS

Iodoethynylbenzene derivatives have proven to be good halogen-bonding donors. The binding of an iodine atom to an sp hybridized carbon atom generates a deep σ-hole in the iodine atom and this, combined with the low steric hindrance of this system, leads to the formation of strong noncovalent interactions with pyridine derivatives (ΔE_{int} = −10 kcal/mol) and somewhat weaker interactions with benzonitriles (ΔE_{int} = −7.5 kcal/mol).

The linear ***p*-BIB** forms halogen-bonding complexes with pyridine-based acceptors bearing one or two aromatic rings to give complexes that show ordered calamitic phases (SmB and G) over wide temperature ranges. On the other hand, the bent m-**BIB** forms halogen-bonding complexes with pyridine derivatives that contain three aromatic rings. These complexes show liquid crystal phases that are characteristic of bent-core compounds, and they respond under electric fields. XRD and modeling studies support the experimental results and also explain the weaker interactions of these iodine donors with a benzonitrile-based acceptor. It was found experimentally that this weaker interaction prevents the formation of homogeneous halogen-bonding complexes on melting.

ACKNOWLEDGMENTS

Dr. Jane Murray of CleveTheoComp LLC (Cleveland) is acknowledged for fruitful discussions. This work was financially supported by MICINN-FEDER of Spain-EU (Projects MAT2009-14636-C03-01, MAT2011-27978-C02-01, CTQ2012-35692 and MAT2012-38538-C03-01) and Aragón Government-FSE (Project E04). The authors acknowledge the Spanish Government for a JAEDoc-CSIC contract (N. Gimeno) and MICINN-FPI fellowship (L. González). Thanks are given to Crystallography Service of the University of Zaragoza (Spain), XPS Service of the Instituto de Nanociencia Aragón, University of Zaragoza (Spain), and Nuclear Magnetic Resonance, Mass Spectrometry and Thermal Analysis Services from the Instituto de Ciencia de Materiales de Aragón, Unversidad de Zaragoza-CSIC (Spain).

REFERENCES

(1) Kato, T.; Frechet, J. M. J. *Liq. Cryst.* **2006**, *33*, 1429−1433.
(2) Kato, T.; Mizoshita, N.; Kishimoto, K. *Angew. Chem., Int. Ed.* **2006**, *45*, 38−68.
(3) Broer, D.; Crawford, G. P.; Zumer, S. *Cross-Linked Liquid Crystalline Systems: From Rigid Polymer Networks to Elastomers*; CRC Press: Boca Raton, FL, 2011.
(4) Kato, T.; Frechet, J. M. J. *J. Am. Chem. Soc.* **1989**, *111*, 8533−8534.
(5) Kato, T.; Wilson, P. G.; Fujishima, A.; Frechet, J. M. J. *Chem. Lett.* **1990**, 2003−2006.
(6) Gimeno, N.; Ros, M. B.; Serrano, J. L.; de la Fuente, M. R. *Angew. Chem., Int. Ed.* **2004**, *43*, 5235−5238.
(7) Barbera, J.; Gimeno, N.; Pintre, I.; Ros, M. B.; Serrano, J. L. *Chem. Commun.* **2006**, 1212−1214.
(8) Perez, A.; Gimeno, N.; Vera, F.; Ros, M. B.; Serrano, J. L.; De la Fuente, M. R. *Eur. J. Org. Chem.* **2008**, 826−833.
(9) Gimeno, N.; Ros, M. B.; Serrano, J. L.; De la Fuente, M. R. *Chem. Mater.* **2008**, *20*, 1262−1271.
(10) Wang, L.-Y.; Chiang, I. H.; Yang, P.-J.; Li, W.-S.; Chao, I. T.; Lin, H.-C. *J. Phys. Chem. B* **2009**, *113*, 14648−14660.
(11) Wang, L.-Y.; Tsai, H.-Y.; Lin, H.-C. *Macromolecules* **2010**, *43*, 1277−1288.
(12) Yang, P.-J.; Wang, L.-Y.; Tang, C.-Y.; Lin, H.-C. *J. Polym. Sci., Part A: Polym. Chem.* **2010**, *48*, 764−774.
(13) Chen, W.-H.; Chuang, W.-T.; Jeng, U. S.; Sheu, H.-S.; Lin, H.-C. *J. Am. Chem. Soc.* **2011**, *133*, 15674−15685.
(14) Guthrie, F. *J. Chem. Soc.* **1863**, 239.
(15) Remses, I.; Norris, J. F. *Am. Chem. J.* **1896**, *18*, 90.
(16) Hassel, O.; Hvoslef, J. *Acta Chem. Scand.* **1954**, *8*, 873−873.
(17) Hassel, O.; Romming, C. *Q. Rev.* **1962**, *16*, 1−18.
(18) Bent, H. A. *Chem. Rev.* **1968**, *68*, 587−648.
(19) Auffinger, P.; Hays, F. A.; Westhof, E.; Ho, P. S. *Proc. Natl. Acad. Sci. U.S.A.* **2004**, *101*, 16789−16794.
(20) Metrangolo, P.; Neukirch, H.; Pilati, T.; Resnati, G. *Acc. Chem. Res.* **2005**, *38*, 386−395.
(21) Voth, A. R.; Ho, P. S. *Curr. Top. Med. Chem.* **2007**, *7*, 1336−1348.
(22) Metrangolo, P.; Meyer, F.; Pilati, T.; Resnati, G.; Terraneo, G. *Angew. Chem., Int. Ed.* **2008**, *47*, 6114−6127.
(23) Metrangolo, P.; Resnati, G. *Halogen Bonding Fundamentals and Applications*; Springer: 2008; Vol. *126*.
(24) Hardegger, L. A.; Kuhn, B.; Spinnler, B.; Anselm, L.; Ecabert, R.; Stihle, M.; Gsell, B.; Thoma, R.; Diez, J.; Benz, J.; Plancher, J. M.; Hartmann, G.; Banner, D. W.; Haap, W.; Diederich, F. *Angew. Chem., Int. Ed.* **2011**, *50*, 314−318.
(25) Nguyen, H. L.; Horton, P. N.; Hursthouse, M. B.; Legon, A. C.; Bruce, D. W. *J. Am. Chem. Soc.* **2004**, *126*, 16−17.
(26) Xu, J. W.; Liu, X. M.; Lin, T. T.; Huang, J. C.; He, C. B. *Macromolecules* **2005**, *38*, 3554−3557.
(27) Xu, J. W.; Liu, X. M.; Ng, J. K. P.; Lin, T. T.; He, C. B. *J. Mater. Chem.* **2006**, *16*, 3540−3545.
(28) Bruce, D. W. In *Halogen Bonding: Fundamentals and Applications*; Metrangolo, P., Resnati, G., Eds.; 2008; Springer: Vol. *126*, pp 161−180.
(29) Bruce, D. W.; Metrangolo, P.; Meyer, F.; Prasang, C.; Resnati, G.; Terraneo, G.; Whitwood, A. C. *New J. Chem.* **2008**, *32*, 477−482.
(30) Bruce, D. W.; Metrangolo, P.; Meyer, F.; Pilati, T.; Prasang, C.; Resnati, G.; Terraneo, G.; Wainwright, S. G.; Whitwood, A. C. *Chem.—Eur. J.* **2010**, *16*, 9511−9524.
(31) Metrangolo, P.; Prasang, C.; Resnati, G.; Liantonio, R.; Whitwood, A. C.; Bruce, D. W. *Chem. Commun.* **2006**, 3290−3292.
(32) Prasang, C.; Whitwood, A. C.; Bruce, D. W. *Chem. Commun.* **2008**, 2137−2139.
(33) Laurence, C.; Queigneccabanetos, M.; Dziembowska, T.; Queignec, R.; Wojtkowiak, B. *J. Am. Chem. Soc.* **1981**, *103*, 2567−2573.
(34) Laurence, C.; Queigneccabanetos, M.; Wojtkowiak, B. *J. Chem. Soc., Perkin Trans. 2* **1982**, 1605−1610.
(35) Laurence, C.; Queigneccabanetos, M.; Wojtkowiak, B. *Can. J. Chem.* **1983**, *61*, 135−138.
(36) Yamamoto, H. M.; Kosaka, Y.; Maeda, R.; Yamaura, J.; Nakao, A.; Nakamura, T.; Kato, R. *ACS Nano* **2008**, *2*, 143−155.
(37) Lieffrig, J.; Yamamoto, H. M.; Kusamoto, T.; Cui, H.; Jeannin, O.; Fourmigue, M.; Kato, R. *Cryst. Growth Des.* **2011**, *11*, 4267−4271.
(38) Sun, A. W.; Lauher, J. W.; Goroff, N. S. *Science* **2006**, *312*, 1030−1034.
(39) Lauher, J. W.; Fowler, F. W.; Goroff, N. S. *Acc. Chem. Res.* **2008**, *41*, 1215−1229.
(40) Luo, L.; Wilhelm, C.; Sun, A.; Grey, C. P.; Lauher, J. W.; Goroff, N. S. *J. Am. Chem. Soc.* **2008**, *130*, 7702−7709.
(41) Lemouchi, C.; Vogelsberg, C. S.; Zorina, L.; Simonov, S.; Batail, P.; Brown, S.; Garcia-Garibay, M. A. *J. Am. Chem. Soc.* **2011**, *133*, 6371−6379.
(42) Kniep, F.; Rout, L.; Walter, S. M.; Bensch, H. K. V.; Jungbauer, S. H.; Herdtweck, E.; Huber, S. M. *Chem. Commun.* **2012**, *48*, 9299−9301.
(43) Ruokolainen, J.; Tanner, J.; Tenbrinke, G.; Ikkala, O.; Torkkeli, M.; Serimaa, R. *Macromolecules* **1995**, *28*, 7779−7784.
(44) Ruokolainen, J.; tenBrinke, G.; Ikkala, O.; Torkkeli, M.; Serimaa, T. *Macromolecules* **1996**, *29*, 3409−3415.
(45) Zhou, X.; Goh, S. H.; Lee, S. Y.; Tan, K. L. *Appl. Surf. Sci.* **1997**, *119*, 60−66.
(46) Wang, F.; Ma, N.; Chen, Q.; Wang, W.; Wang, L. *Langmuir* **2007**, *23*, 9540−9542.
(47) Priimagi, A.; Cavallo, G.; Forni, A.; Gorynsztejn-Leben, M.; Kaivola, M.; Metrangolo, P.; Milani, R.; Shishido, A.; Pilati, T.; Resnati, G.; Terraneo, G. *Adv. Funct. Mater.* **2012**, *22*, 2572−2579.
(48) Barres, A. L.; El-Ghayoury, A.; Zorina, L. V.; Canadell, E.; Auban-Senzier, P.; Batail, P. *Chem. Commun.* **2008**, 2194−2196.
(49) Eremin, A.; Diele, S.; Pelzl, G.; Nadasi, H.; Weissflog, W.; Salfetnikova, J.; Kresse, H. *Phys. Rev. E* **2001**, *64*, 051707−051712.
(50) Sadashiva, B. K.; Reddy, R. A.; Pratibha, R.; Madhusudana, N. V. U. *Mater. Chem.* **2002**, *12*, 943−950.
(51) Pociecha, D.; Cepic, M.; Gorecka, E.; Mieczkowski, J. *Phys. Rev. Lett.* **2003**, *91*, 185501−185504.

(52) Reddy, R. A.; Sadashiva, B. K. *J. Mater. Chem.* **2004**, *14*, 310−319.
(53) Shimbo, Y.; Gorecka, E.; Pociecha, D.; Araoka, F.; Goto, M.; Takanishi, Y.; Ishikawa, K.; Mieczkowski, J.; Gomola, K.; Takezoe, H. *Phys. Rev. Lett.* **2006**, *97*, 113901−113904.
(54) Gomola, K.; Guo, L.; Pociecha, D.; Araoka, F.; Ishikawa, K.; Takezoe, H. *J. Mater. Chem.* **2010**, *20*, 7944−7952.
(55) Guo, L.; Dhara, S.; Sadashiva, B. K.; Radhika, S.; Pratibha, R.; Shimbo, Y.; Araoka, F.; Ishikawa, K.; Takezoe, H. *Phys. Rev. E* **2010**, *81*, 11703.
(56) Tsuzuki, S.; Wakisaka, A.; Ono, T.; Sonoda, T. *Chem.—Eur. J.* **2012**, *18*, 951−960.
(57) Wendler, K.; Thar, J.; Zahn, S.; Kirchner, B. *J. Phys. Chem. A* **2010**, *114*, 9529−9536.